Electronic Supplementary Information (ESI)
Phase matching achieved by isomorphous substitution in IR nonlinear optical material $Ba_2SnSSi_2O_7$ with an undiscovered [SnO_4S] functional motif

Yong-Fang Shi,‡[a,b] Zuju Ma,‡[c] Bing-Xuan Li,[a,b] Xin-Tao Wu,[a,b] Hua Lin,*[,a,b] and Qi-Long Zhu*,[a,b]

[a]*State Key Laboratory of Structural Chemistry, Fujian Institute of Research on the Structure of Matter, Chinese Academy of Sciences, Fuzhou 350002, China*

[b]*Fujian Science & Technology Innovation Laboratory for Optoelectronic Information of China, Fuzhou, Fujian 350108, China*

[c]*School of Environmental and Materials Engineering, Yantai University, Yantai 264005, China*

‡Y. F. S. and Z. M. contributed equally to this work.

Table of Contents

Electronic Supplementary Information (ESI)

Electronic Supplementary Information (ESI)

1 Experimental Section

1.1 Materials and Instruments

All reagents used in the present experiments were purchased from commercial sources and directly used without further purification. All weighing processes were completed in an anhydrous and oxygen-free glove box. The semi-quantitative energy dispersive X-ray (EDX, Oxford INCA) spectra were measured with a field emission scanning electron microscope (FESEM, JSM6700F). Powder X-ray diffraction (PXRD) analysis was carried out in a Rigaku Mini-Flex II powder diffractometer (Cu-K_α, λ = 1.5418 Å). UV-vis-NIR absorption measurement was performed in the region of 200−2500 nm at room temperature using an UV-vis-NIR spectrometer (Perkin-Elmer Lambda 950). The reflectance spectrum of the $BaSO_4$ powder was collected as the baseline and the diffuse reflectance data were converted to absorbance internally by the instrument by use of the Kubelka-Munk function.[1] The IR transmittance was measured on the PerkinElmer Spectrum One FT-IR Spectrometer in the range of 400−4000 cm^{-1}. The thermal stability analyses were measured on a NETZSCH STA 449C simultaneous analyser. The birefringence (Δn) was characterized by using the polarizing microscope (ZEISS Axio Scope, A1) equipped with Berek compensator. The wavelength of the light source was 546 nm. The formula for calculating the Δn is $R = | N_e – N_o | \times T = \Delta n \times T$. Here, R represents the optical path difference and T denotes the thickness of the crystal.

Electronic Supplementary Information (ESI)

1.2 Synthesis

In this work, BaO (4 N), BaS (4 N), SnO_2 (4 N), SiO_2 (3 N), and KBr (3 N) were used as raw materials without further purification. A mixture of BaO (1 mmol), BaS (1 mmol), SnO_2 (1 mmol), SiO_2 (2 mmol), and KBr (2 mmol) was sealed into an evacuated silica tube and subjected to the following heat treatment: quickly heated to 923K in 10hours, held at this temperature for 10 hours, next, quickly heated to 1123K in 10 hours, held at this temperature for 72 hours, then and cooled to ambient conditions at 6 K/h. Finally, the colorless single crystals of $Ba_2SnSi_2O_7S$ with a high yield of 90% (based on Sn) were obtained in air after washed with deionized water and dried with ethanol.

1.3 Single-Crystal Structure determination

Taking some high-quality crystals of $Ba_2SnSSi_2O_7$with suitable sizes were selected for single-crystal X-ray diffraction (XRD) analysis. The single-crystal diffraction data collections were collected on a Saturn 724 install with graphite-monochromated Mo-K_α radiation (λ = 0.71073 Å) at room temperature.The absorption correction was performed by the multi-scan method.[2] Using direct methods and maken further refinement by full-matrix least-square fitting on F^2 based on *SHELX−2014* software, the precise struture was determined sussessfully.[3] Crystallographic data and refinement details are given in the Table S1. The atomic coordinates and equivalent isotropic of crystallographic information displacement parameters are given in the Table S2. Bond distances (Å) and bond angles (°) of $Ba_2SnSSi_2O_7$ are listed in Table S3. CIFs of $Ba_2SnSSi_2O_7$ have been submitted with CCDC numbers 2155594.

1.4 Second-Harmonic Generation (SHG) Measurements

According to Kurtz-Perry method, the powder SHG property measurement was performed in 2050 nm and 1064 nm Q-switch laser radiation (laser energy is 10mJ).

$AgGaS_2$ (high quality single crystals as reference material were provided by Anhui Institute of Optics and Fine Mechanics Chinese Academy of Sciences) and KDP were taken as contrast material in the same condition, respectively.[4] The different granule size scopes (30−46, 46−74, 74−106, 106−150, 150−210 μm) of $Ba_2SnSSi_2O_7$, $AgGaS_2$ and KDP were ground and screen out. The SHG intensity of the frequency-doubled output gave out the prepared materials were observed via a photomultiplier tube and saved on the oscilloscope.

1.5 Laser Induced Damage Threshold (LIDT) Measurements

The LIDT of $Ba_2SnSSi_2O_7$ at the maximal scope of 150−210 μm was carried out single pulse measurement method[5] and similar scope of $AgGaS_2$ and KDP single crystals used to the references. The whole measuring materials were foist into selfsame plastic holders (thickness: 1 mm and diameter: 8 mm), respectively. Using an optical microscope monitor the exterior change of sample under the 1064 nm laser radiation with pulse width τ_p of 10 ns. Nova II sensor with a PE50-DIF-C energy sensor and a Vernier caliper was used for measuring the power of laser beam and the damage spot radius.

2 Computational Details

The DFT calculations have been performed using the *Vienna ab initio simulation package* (VASP)[6–8] with the Perdew-Burke-Ernzerhof (PBE)[9] exchange correlation functional. The projected augmented wave (PAW)[10] potentials with the valence states 5s, 5p and 6s for Ba, 5s and 5p for Sn, 3s and 3p for Si, 3s and 3p for S, and 2s and 2p for O, respectively, have been used. A Γ-centered 7×7×9 Monkhorst-Pack grid for the Brillouin zone sampling[11] and a cutoff energy of 750 eV for the plane wave expansion were found to get convergent lattice parameters. The linear and nonlinear optical

calculation was performed in the condition of a Monkhorst-Pack *k*-point mesh of 7×9×9.

The imaginary part of the dielectric function due to direct inter-band transitions is given by the expression:

$$\varepsilon_2(\hbar\omega) = \frac{2e^2\pi}{\Omega\varepsilon_0}\sum_{k,v,c}\left|\left\langle\psi_k^c\left|u\cdot r\right|\psi_k^v\right\rangle\right|^2\delta(E_k^c - E_k^v - E) \quad \ldots\ldots\ldots\ldots (1)$$

where Ω, ω, u, v and c are the unit-cell volume, photon frequencies, the vector defining the polarization of the incident electric field, valence and conduction bands, respectively. The real part of the dielectric function is obtained from ε_2 by a Kramers-Kronig transformation:

$$\varepsilon_1(\omega) = 1 + (\frac{2}{\pi})\int_0^{+\infty} d\omega' \frac{\omega'^2\varepsilon_2(\omega)}{\omega'^2 - \omega^2} \quad \ldots\ldots\ldots\ldots (2)$$

The refractive index $n(\omega)$ can be obtained based on ε_1 and ε_2.

In calculation of the static $\chi^{(2)}$ coefficients, the so-called length-gauge formalism[12] derived by Aversa and Sipe[13] and modified by Rashkeev et al[14] is adopted, which has proven to be successful in calculating the second order susceptibility for semiconductors and insulators. In the static case, the imaginary part of the static second-order optical susceptibility can be expressed as:

$$\begin{aligned}\chi^{abc} &= \frac{e^3}{\hbar^2\Omega}\sum_{nml,k}\frac{r_{nm}^a(r_{ml}^b r_{ln}^c + r_{ml}^c r_{ln}^b)}{2\omega_{nm}\omega_{ml}\omega_{ln}}[\omega_n f_{ml} + \omega_m f_{ln} + \omega_l f_{nm}] \\ &+ \frac{ie^3}{4\hbar^2\Omega}\sum_{nm,k}\frac{f_{nm}}{\omega_{mn}^2}[r_{nm}^a(r_{mn;c}^b + r_{mn;b}^c) + r_{nm}^b(r_{mn;c}^a + r_{mn;a}^c) + r_{nm}^c(r_{mn;b}^a + r_{mn;a}^b)]\end{aligned}$$

……(3)

where r is the position operator, $\hbar\omega_{nm} = \hbar\omega_n - \hbar\omega_m$ is the energy difference for the bands m and n, $f_{mn} = f_m - f_n$ is the difference of the Fermi distribution functions,

subscripts *a*, *b*, and *c* are Cartesian indices, and $r^{b}_{mn;a}$ is the so-called generalized derivative of the coordinate operator in *k* space,

$$r^{b}_{nm;a} = \frac{r^{a}_{nm}\Delta^{b}_{mn} + r^{b}_{nm}\Delta^{a}_{mn}}{\omega_{nm}} + \frac{i}{\omega_{nm}} \times \sum_{l} (\omega_{lm} r^{a}_{nl} r^{b}_{lm} - \omega_{nl} r^{b}_{nl} r^{a}_{lm}) \quad \ldots\ldots\ldots\ldots (4)$$

where $\Delta^{a}_{nm} = (p^{a}_{nn} - p^{a}_{mm}) / m$ is the difference between the electronic velocities at the bands *n* and *m*.

As the nonlinear optical coefficients is sensitive to the momentum matrix, much finer k-point grid and large amount of empty bands are required to obtain a convergent $\chi^{(2)}$ coefficient. The $\chi^{(2)}$ coefficients here were calculated from PBE wave functions and a scissor operator has been added to correct the conduction band energy (corrected to the experimental gap), which has proven to be reliable in predicting the second order susceptibility for semiconductors and insulators.

Electronic Supplementary Information (ESI)

3 Figures and Tables

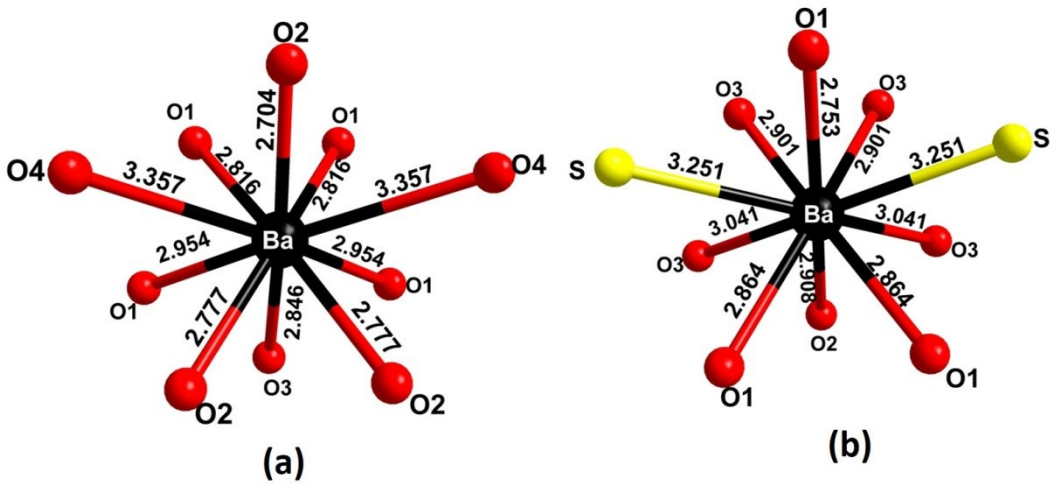

Figure S1. The coordination environment and bond lengths (Å) of crystallographic independent Ba atoms in (a)$Ba_2TiOSi_2O_7$ and (b)$Ba_2SnSSi_2O_7$.

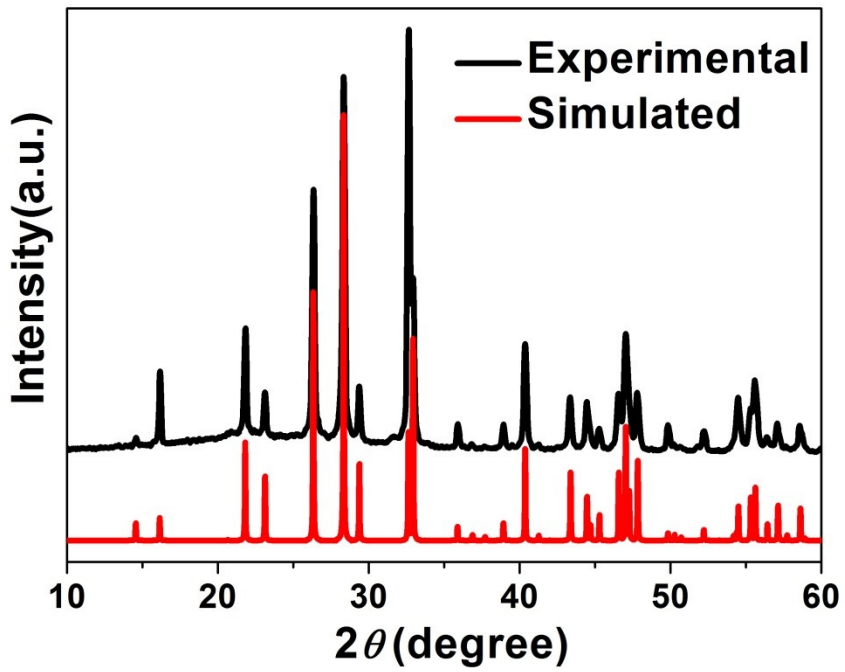

Figure S2. Experimental (black) and simulated (red) powder XRD patterns of $Ba_2SnSSi_2O_7$.

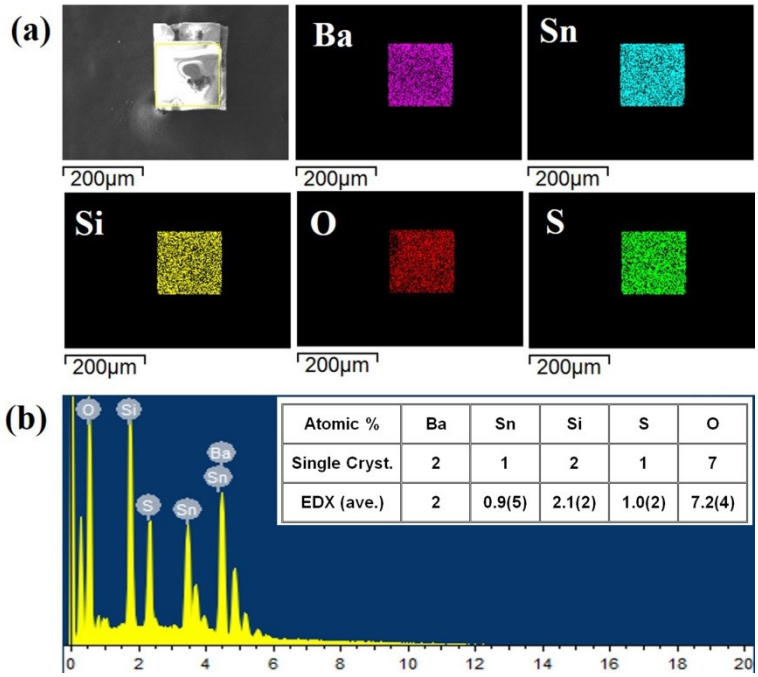

Figure S3. The characterizations of $Ba_2SnSSi_2O_7$: (a) SEM image and corresponding elemental mapping analysis and (b) EDX results.

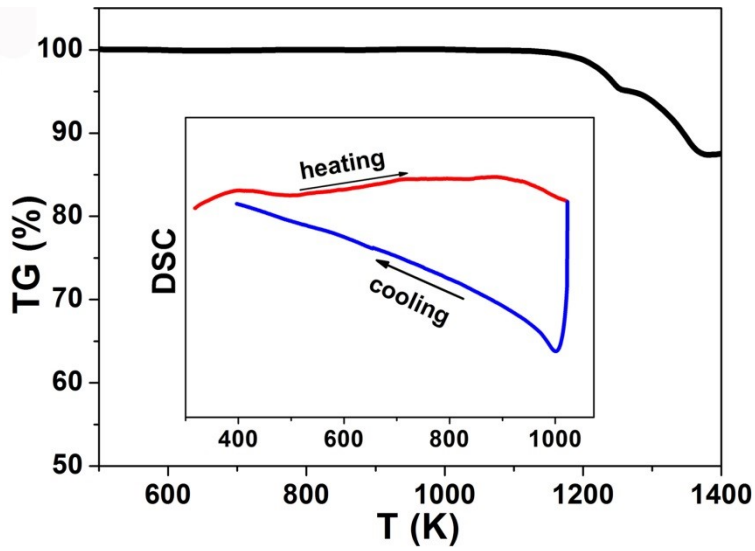

Figure S4. TG diagram (inset: DSC cyclic curves) of $Ba_2SnSSi_2O_7$.

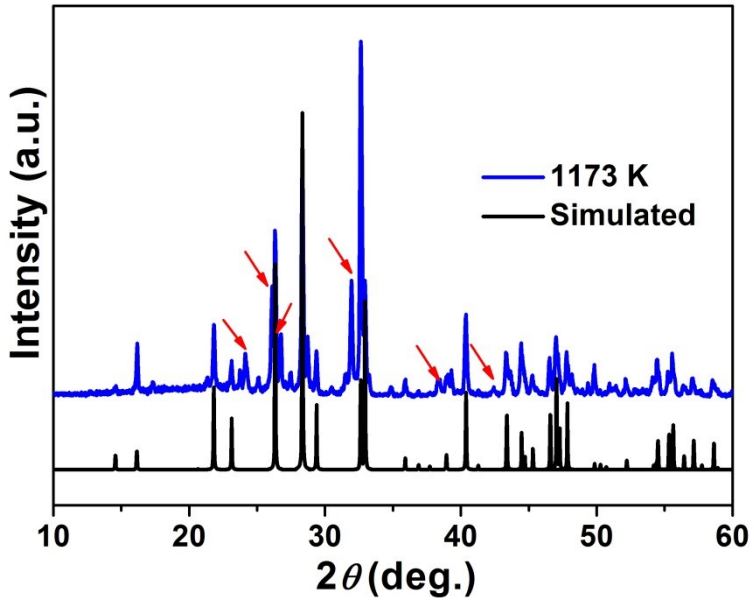

Figure S5. The PXRD of experimental $Ba_2SnSSi_2O_7$ calcining in 1173 K (blue), simulated $Ba_2SnSSi_2O_7$ (black), and $BaSiO_3$ (PDF#:70-2112) (red arrow) .

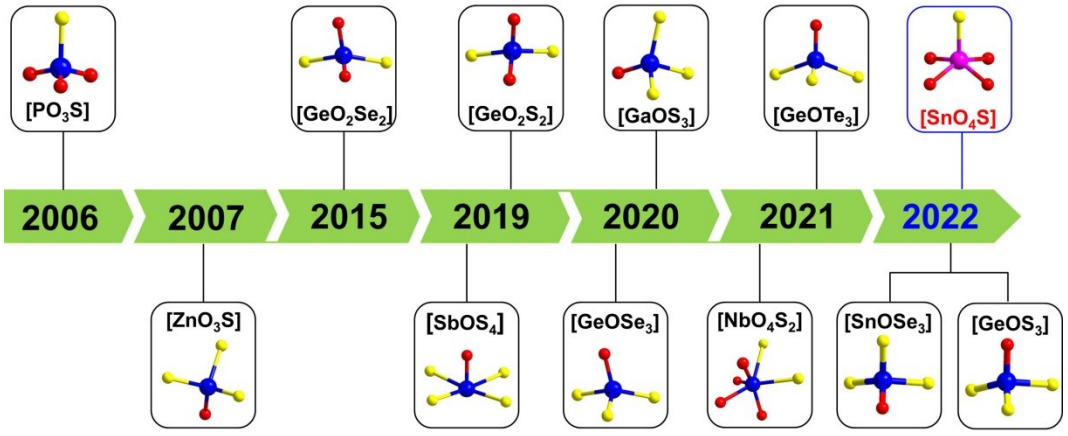

Figure S6. Timeline of mixed-anion NLO-active motifs reported in NCS oxychalcogenides.

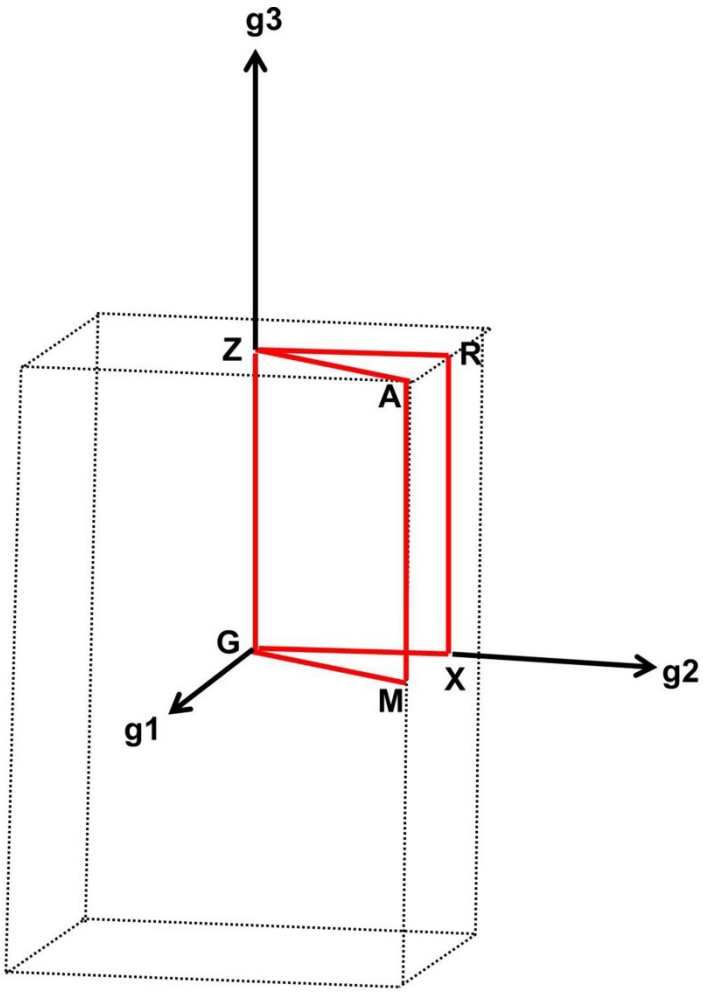

Figure S7. The first Brillouin zone with high symmetry points for $Ba_2SnSSi_2O_7$.

Electronic Supplementary Information (ESI)

Table S1. Crystallographic data and refinement details for $Ba_2SnSSi_2O_7$.

Empirical formula	$Ba_2SnSSi_2O_7$
Formula weight	593.61
Temperature(K)	293(2)
Crystal size (mm)	0.25 × 0.2 × 0.2
Crystal system	Tetragonal
Space group	*P*4*bm* (No.100)
a (Å)	8.5915(3)
b (Å)	8.5915(3)
c (Å)	5.4835(4)
V (Å^3)	404.76(4)
Z	2
D_c (g·cm^{-3})	4.871
μ (mm^{-1})	13.237
GOOF on F^2	1.005
R_1, wR_2 ($I > 2\sigma(I)$) [a]	0.0142, 0.0360
R_1, wR_2 (all data)	0.0142, 0.0360
Largest diff. peak and hole (e·Å^{-3})	0.542, –0.518
Flack parameter	0.06(2)

Table S2. Atomic coordinates and equivalent isotropic displacement parameters of $Ba_2SnSSi_2O_7$.

Atom	*Wyckff*	*x*	*y*	*z*	U_{eq}(Å)[a]
Ba	4*c*	0.32840(3)	0.82840(3)	0.12052(11)	0.00531(18)
Sn	2*a*	0	0	0.57697(12)	0.0063(2)
Si	4*c*	0.87354(15)	0.37354(15)	0.6044(5)	0.0059(4)
S	2*a*	0	0	0	0.0071(5)
O1	4*c*	0.8742(5)	0.3742(5)	0.8956(11)	0.0059(10)
O2	2*b*	0.5	0	0.4901(16)	0.0186(19)
O3	8*d*	0.7880(5)	0.9223(6)	0.4693(9)	0.0223(11)

U_{eq} is defined as one third of the trace of the orthogonalized U_{ij} tensor.

Table S3. Selected bond lengths (Å) and angle (°) of $Ba_2SnSSi_2O_7$.

Sn–S3×4	2.028(5)	∠ O3–Sn–O3×2	146.1(3)
Sn–S	2.320(3)	∠ O3–Sn–O3×4	85.13(8)
Si–O1	1.597(6)	∠ O3–Sn–S×4	106.94(13)
Si–O3×2	1.628(8)	∠O1–Si–O3×2	117.2(2)
Si–O1	1.659(4)	∠O3–Si–O3	103.4(4)
Ba–O1×2	2.865(4)	∠O3–Si–O2×2	102.6(3)
Ba–O1	2.753(6)	∠O3–Si–O3	111.9(4)
Ba–O3×2	2.901(5)		
Ba–O3×2	3.041(5)		
Ba–S×2	3.2513(6)		

Table S4. Properties comparison of the reported NLO oxychalcogenides.

Compounds	Space group	E_g (eV)	d_{eff}	PM/NPM	Ref.
α-Na_3PO_3S	*R*3*c* (No. 161)	N/A	200 × SiO_2	NPM	15
$Sr_4Pb_{1.5}Sb_5O_5Se_8$	*Cm* (No. 8)	0.92	0.25 × $AgGaS_2$	N/A	16
$Sr_6Cd_2Sb_6O_7S_{10}$	*Cm* (No. 8)	1.89	4 × $AgGaS_2$	PM	17
$Ba_3Ge_2O_4Te_3$	*R*3*m* (No. 160)	2.08	0.6× $AgGaSe_2$	PM	18
$Sm_3NbS_3O_4$	*Pna*2$_1$ (No. 33)	2.68	0.3 × $AgGaS_2$	PM	19
$Gd_3NbS_3O_4$	*Pna*2$_1$ (No. 33)	2.74	0.4 × $AgGaS_2$	PM	19
$Sr_3Ge_2O_4Se_3$	*R*3*m* (No. 160)	2.96	0.8 × $AgGaS_2$	PM	20
$SrGeOSe_2$	*P*2$_1$2$_1$2$_1$ (No. 19)	3.16	1.3 × $AgGaS_2$	PM	21
$BaGeOSe_2$	*P*2$_1$2$_1$2$_1$ (No. 19)	3.2	1.1 × $AgGaS_2$	PM	22
$Sr_3[SnOSe_3][CO_3]$	*Pna*2$_1$ (No. 33)	3.16	1.0 × $AgGaS_2$	PM	23
$Sr_2MnGe_2OS_6$	*P*$\bar{4}$2$_1$*m* (No. 113)	3.51	0.3 × $AgGaS_2$	PM	24
$Sr_2CdGe_2OS_6$	*P*$\bar{4}$2$_1$*m* (No. 113)	3.62	0.8 × $AgGaS_2$	PM	24
$Sr_2ZnGe_2OS_6$	*P*$\bar{4}$2$_1$*m* (No. 113)	3.73	0.6 × $AgGaS_2$	PM	24
CaZnOS	*P*6$_3$*mc* (No. 186)	3.71	100 × SiO_2	NPM	25
$SrZn_2OS_2$	*Pmn*2$_1$ (No. 31)	3.86	2 × KDP	PM	26
$Sr_5Ga_8O_3S_{14}$	*P*2$_1$2$_1$2 (No. 18)	3.9	0.8 × $AgGaS_2$	NPM	27
$SrGeOS_2$	*P*2$_1$2$_1$2$_1$ (No. 19)	3.9	0.4 × $AgGaS_2$	NPM	28
$Ba_2SnSSi_2O_7$	***P4bm* (No. 100)**	**4.05**	**0.6 × $AgGaS_2$**	**PM**	**This Work**
$BaGeOS_2$	*P*2$_1$2$_1$2$_1$ (No. 19)	4.1	0.5 × $AgGaS_2$	NPM	28
$La_3Ga_3Ge_2S_3O_{10}$	*P*$\bar{6}$2*c* (No. 190)	4.7	2 × KDP	PM	29

Table S5. The static SHG coefficients d_{ij} (pm/V) for $Ba_2SnSSi_2O_7$ and $Ba_2TiOSi_2O_7$.

Compounds	$Ba_2SnSSi_2O_7$	$Ba_2TiOSi_2O_7$
d_{ij} (pm/V) at 2050 nm	$d_{31} = 1.030$	$d_{31} = 0.721$
	$d_{32} = 1.034$	$d_{32} = 0.724$
	$d_{33} = 2.95$	$d_{33} = 2.06$

4 References

1 P. Kubelka and F. Munk, Reflection characteristics of paints. *Z. Techn. Phys.*, 1931, **12**, 593−601.

2 CrystalClear Version 1.3.5; Rigaku Corp.: Woodlands, TX, 1999.

3 P. Kubelka, Ein beitrag zur optik der farbanstriche. *Z. Tech. Phys.*, 1931, **12**, 593–601.

4 S. K. Kurtz and T. T. Perry, A powder technique for the evaluation of nonlinear optical materials. *J. Appl. Phys.*, 1968, **39**, 3798−3813.

5 M. J. Zhang, X. M. Jiang, L. J. Zhou and G. C. Guo, Two phases of Ga_2S_3: promising infrared second-order nonlinear optical materials with very high laser induced damage thresholds. *J. Mater. Chem. C*, 2013, **1**, 4754–4760.

6 G. Kresse, VASP, 5.3.5; http://cms.mpi.univie.ac.at/vasp/vasp/vasp.html.

7 G. Kresse and J. Furthmuller, Efficient iterative schemes for ab initio total-energy calculations using a plane-wave basis set. *Phys. Rev. B: Condens. Matter*, 1996, 11169–11186.

8 G. Kresse and D. Joubert, From ultrasoft pseudopotentials to the projector augmented-wave method. *Phys. Rev. B: Condens. Matter*, 1999, **59**, 1758–1775.

9 P. E. Blochl, Projector augmented-wave method. *Phys. Rev. B: Condens. Matter*, 1994, **50**, 17953–17979.

10 J. P. Perdew, K. Burke and M. Ernzerhof, Generalized gradient approximationmade simple. *Phys. Rev. Lett.*, 1996, **77**, 3865–3868.

11 D. J. Chadi, Special points for Brillouin-zone integrations. *Phys. Rev. B: Condens. Matter*,1976, **16**, 1746–1747.

12 Z.Fang, J. Lin, R. Liu, P. Liu, Y. Li, X. Huang, K. Ding, L. Ning and Y. Zhang, Computational design of inorganic nonlinear optical crystals based on a genetic algorithm. *CrystEngComm*, 2014, **16**, 10569–10580.

13 C. Aversa and J. E. Sipe, Nonlinear optical susceptibilities of semiconductors: Results with a length-gauge analysis. *Phys. Rev. B*, 1995, **52**, 14636–14645.

14 S. N. Rashkeev and W. R. L. Lambrecht, B. Segall, Efficient ab initio method for the calculation of frequency-dependent second-order optical response in semiconductors. *Phys. Rev. B*, 1998, **57**, 3905–3919.

15 N. J. Takas and J. A. Aitken, Phase transitions and second-harmonic generation in sodium monothiophosphate. *Inorg. Chem*., 2006, **45**, 2779–2781.

16 Y. Wang, M. J. Luo, P. Zhao, X. L. Che, Y. Z. Cao and F. Q. Huang, $Sr_4Pb_{1.5}Sb_5O_5Se_8$: a new mid-infrared nonlinear optical material with a moderate SHG response. *CrystEngComm*, 2020, **22**,3526–3530.

17 R. Wang, F. Liang, F. Wang, Y. Guo, X. Zhang, Y. Xiao, K. Bu, Lin, Z.; Yao, J.; T. Zhai and F. Huang, $Sr_6Cd_2Sb_6O_7S_{10}$: Strong SHG Response Activated by Highly Polarizable Sb/O/S Groups. *Angew. Chem. Int. Ed*., 2019, **24**, 8078–8081.

18 M. Sun, X. Zhang, C. Li, W. Liu, Z. Lin and J. Yao, Highly polarized [$GeOTe_3$] motif-driven structural order promotion and an enhanced second harmonic generation response in the new nonlinear optical oxytelluride $Ba_3Ge_2O_4Te_3$. *J. Mater. Chem. C*, 2021, **10**, 150–159.

19 X. Lian, Z.-T. Lu, W.-D. Yao, S.-H.Yang, W. Liu, R.-L.Tang and S.-P. Guo, Structural Transformation and Second-Harmonic-Generation Activity in Rare-Earth and d^0 Transition-Metal Oxysulfides $RE_3NbS_3O_4$ (RE = Ce, Sm, Gd, Dy). *Inorg. Chem.*, 2021, **60**, 10885–10889.

20 W. H. Xing, P. Fang, N. Z. Wang, Z. Li, Z. S. Lin, J. Y. Yao, W. L.Yin and B. Kang, Two Mixed-Anion Units of [$GeOSe_3$] and [GeO_3S] Originating from Partial Isovalent Anion Substitution and Inducing Moderate Second Harmonic Generation Response and Large Birefringence. *Inorg. Chem*., 2020, **59**, 16716–16724.

21 M.-Y. Ran, Z. Ma, H. Chen, B. Li, X.-T. Wu, H. Lin and Q.-L. Zhu, Partial Isovalent Anion Substitution to Access Remarkable Second-Harmonic Generation Response: A Generic and Effective Strategy for Design of Infrared Nonlinear Optical Materials. *Chem. Mater*., 2020, **32**, 5890–5896.

22 B.-W. Liu, X.-M. Jiang, G.-E Wang, H.-Y. Zeng, M.-J. Zhang, S.-F. Li, W.-H.Guo and G.-C. Guo, Oxychalcogenide $BaGeOSe_2$: Highly Distorted Mixed-Anion Building Units Leading to a Large Second-Harmonic Generation Response.*Chem. Mater*., 2015, **27**, 8189–8192.

23 J. K. Wang, Y. S. Cheng, H. P. Wu, Z. G. Hu, J. Y. Wang, Y. C. Wu and H. W. Yu, $Sr_3[SnOSe_3][CO_3]$: A Heteroanionic Nonlinear Optical Material Containing Planar π-conjugated [CO_3] and Heteroleptic [$SnOSe_3$] Anionic Groups. *Angew. Chem. Int. Ed.*, 2022, e202201616.

24 M.-Y. Ran, S.-H. Zhou, B. X. Li, W. B. Wei, X.-T. Wu, H. Lin and Q.-L. Zhu, Enhanced Second-Harmonic-Generation Efficiency and Birefringence in Melillite Oxychalcogenides $Sr_2MGe_2OS_6$ (M = Mn, Zn, and Cd). *Chem. Mater.*, 2022, DOI: 10.1021/acs.chemmater.2c00385.

25 T. Sambrook, C. F. Smura, S. J. Clarke, K. M.Ok and P. S. Halasyamani, Structure and physical properties of the polar oxysulfide CaZnOS. *Inorg. Chem*., 2007, **46**, 2571–2574.

26 Y.T sujimoto, C. A. Juillerat, W. Zhang, K. Fujii, M. Yashima, P. S. Halasyamani and H. C. Zurloye, Function of Tetrahedral ZnS_3O Building Blocks in the Formation of $SrZn_2S_2O$: A Phase Matchable Polar Oxysulfide with a Large Second Harmonic Generation Response.*Chem. Mater*., 2018, **30**, 6486–6493.

27 R. Wang, Y. Guo, X. Zhang, Y. Xiao, J. Yao and F. Huang, $Sr_5Ga_8O_3S_{14}$: A Nonlinear Optical Oxysulfide with Melilite-Derived Structure and Wide Band Gap. *Inorg. Chem*., 2020, **59**, 9944–9950.

28 X. Zhang, Y. Xiao, R.Wang, P. Fu, C. Zheng and F. Huang, ynthesis, crystal structures and optical properties of noncentrosymmetric oxysulfides $AeGeS_2O$ (Ae = Sr, Ba). *Dalton Trans*., 2019, **48**, 14662–14668.

29 H. Yan, Y. Matsushita, K.Yamaura and Y.Tsujimoto, $La_3Ga_3Ge_2S_3O_{10}$: An Ultraviolet Nonlinear Optical Oxysulfide Designed by Anion-Directed Band Gap Engineering. *Angew. Chem. Int. Ed.*, 2021, **60**, 26561–26565.